Oxidative dehydrogenation of ethylbenzene over $Cu_{1-x}Co_xFe_2O_4$ catalyst system: influence of acid–base property

Thomas Mathew, Sachin Malwadkar, Shivanand, Pai, N. Sharanappa, C.P. Sebastian, C.V.V. Satyanarayana, and V.V. Bokade*

Catalysis Division, National Chemical Laboratory, Pune 411 088, India

Received 26 June 2003; accepted 29 September 2003

A series of Cu–Co ferrites with the general formula $Cu_{1-x}Co_xFe_2O_4$ ($x = 0$, 0.25, 0.50, 0.75 and 1.0) was prepared by a low-temperature hydroxide coprecipitation route. The catalyst systems were characterized by adopting various physicochemical techniques. The acid–base properties were studied in detail, and the catalytic activity as well as the selectivity for oxidative dehydrogenation of ethylbenzene was compared for various compositions. FTIR adsorption of pyridine is carried out to understand the relative acidity of various compositions of the systems. IR studies of spinel surface with adsorbed CO_2 and adsorption studies of electron acceptors such as 7,7,8,8-tetracyanoquinodimethane, 2,3,5,6-tetrachloro-1-4-benzoquinone and *p*-dinitrobenzene are carried out to evaluate the nature of basic sites and the strength and distribution of electron donor sites present on the spinel surface. It is found that acidity (basicity) of the $Cu_{1-x}Co_xFe_2O_4$ spinel system increases (decreases) from $x = 0$ to 1. A good correlation was found between the activity for this reaction and the surface acid–base properties of the catalysts. Intermediate compositions show better catalytic performance, among which $x = 0.50$ is superior and demonstrates an intermediate acid–base character. It was observed that dehydrogenation of ethylbenzene to styrene proceeds mainly on an acid–base pair site.

KEY WORDS: spinel; ferrites; $Cu_{1-x}Co_xFe_2O_4$; ethylbenzene; dehydrogenation; acid–base properties.

1. Introduction

The catalytic dehydrogenation of ethylbenzene is of industrial importance in the manufacture of styrene as it is extensively used as an intermediate for the manufacture of polystyrene [1–3]. Styrene is manufactured industrially by the dehydrogenation of ethylbenzene over iron oxide promoted by alkali metal ions [1–3]. A lot of reports are available on ethylbenzene dehydrogenation reaction over a variety of mixed oxides, such as K-promoted iron oxide [1], iron oxide containing trace amounts of cerium oxide and molybdenum oxide [4–5], TiO_2-ZrO_2 [6–7], titania [8] etc. Iron oxide catalyst is known to be favorable in the synthesis of styrene but has a low activity [1]. In order to improve their catalytic performance, several kinds of components were doped into Fe_2O_3 [4,5]. Addition of other metal ions to the iron oxide system modifies the acid–base properties of the system and brings out substantial change in the ethylbenzene dehydrogenation activity. For example, both Cu^{2+} and Co^{2+} ions have got diverse character with respect to their activity toward the reaction involving H_2; the former is a dehydrogenating agent, whereas the latter is a hydrogenating agent. The hydrogenation/dehydrogenation ability of these ions is very important in reactions involving decomposition of alcohols, dehydrogenation of aliphatic and aromatic compounds etc. [9–11]. It is also to be emphasized here that the Cu–Co mixed system can act as a dual reaction catalyst depending on the material preparation and reaction conditions [12].

Spinel oxides, having cation distribution in two crystallographic environments [13], are reported to have more activity for the dehydrogenation of hydrocarbon [9], isopropanol [14] and cyclohexanol [15]. Ferrites, a subgroup of spinels, are very much effective for many of those reactions as mentioned above. The catalytic effectiveness of ferrites for many such reactions arises because of the ease with which iron can exchange its oxidation state between 2 and 3. Another important attribute of these materials, from commercial standpoint, is their stability under extremely reducing conditions, which is due to the spinel structure. Thus, the reduction of Fe^{3+} to Fe^{2+} takes place without altering the lattice configurations so that upon reoxidation, the original state is retained [16]. In contrast to the spinel ferrites, the catalyst Fe_2O_3 loses its activity as it is reduced to FeO and metallic iron.

Though a wide variety of mixed oxides have been tried for ethylbenzene dehydrogenation, only very few reports are available on mixed oxides based on spinel type system [17,18]. Also, only a few studies have been reported regarding correlation between acid–base property and ethylbenzene dehydrogenation activity [6–8]. In the present study, the effects of the simultaneous addition of copper and cobalt are studied in a series of $Cu_{1-x}Co_xFe_2O_4$ ($x = 0$, 0.25, 0.50, 0.75 and 1) samples.

* To whom correspondence should be addressed.
E-mail: bokade@cata.ncl.res.in

1011-372X/03/1200–0217/0

We present the results obtained in the oxidative dehydrogenation of ethylbenzene with various compositions of Cu–Co ferrite systems and compare the influence on activity in terms of ethylbenzene conversion and styrene selectivity with the acid–base properties of the ferrospinel system.

2. Experimental

2.1. Catalyst preparation

A series of $Cu_{1-x}Co_xFe_2O_4$ samples ($x = 0$, 0.25, 0.50, 0.75 and 1.0) was prepared by a low-temperature-controlled coprecipitation method using aqueous solutions of ferric nitrate (2.6 M), copper nitrate (3.4 M), cobalt nitrate (3.4 M) and sodium hydroxide (5.3 M). The metal ion solutions were premixed in the required stoichiometric ratio and rapidly added to sodium hydroxide solution. The precipitate was separated and washed free off nitrate and sodium ions with demineralized water. The washed precipitate was initially dried in air at 353 K for about 36 h. The dried materials were powdered and calcined at 773 K. Catalyst pellets of the required mesh size were then obtained by pressing under 10 torr of pressure.

2.2. Physicochemical characterization

The chemical compositions of the calcined catalysts were determined by X-ray fluorescence (XRF) and found to be in line with the starting composition. XRD patterns were recorded with a Rigaku Geigerflex instrument using Cu Kα radiation ($\lambda = 0.15405$ nm) with a nickel filter. The BET surface area and pore volume of the different compositions of the ferrite systems were determined by an N_2-adsorption–desorption method at 77 K using a Quantachrome Nova-1200 adsorption unit (table 1). The IR spectra of the ferrite samples were recorded by a diffuse reflectance (DR) method (Shimadzu, model 8300) between 400 and 1000 cm^{-1}.

2.3. Evaluation of surface acidity and basicity

FTIR adsorption of pyridine is carried out to understand the relative acidity of various compositions. Pyridine adsorption is carried out in drift mode and the detailed experimental procedure is given elsewhere [19].

For basicity, two independent methods have been carried out viz., FTIR adsorption of CO_2 and adsorption studies using different electron acceptors. Adsorption studies were carried out over 0.5-g calcined sample placed in a cylindrical glass vessel fitted with a mercury-sealed stirrer. The catalysts were activated at 773 K for 2 h prior to each experiment. Before sealing, the sample was outgassed at 10 torr for 1 h. Then, the catalyst was suspended in a 10 mL solution of an electron acceptor in acetonitrile. Stirring was continued for 4 h in a mechanically driven stirrer at 300 K in a thermostated bath, and the oxide was collected by centrifuging the solution. The amount of electron acceptor adsorbed was determined from the difference in the adsorption of electron acceptor solution before and after adsorption, which was measured by means of a Shimadzu UV–vis spectrophotometer (λ_{max} of electron acceptors in solvent: 393.5 nm for TCNQ, 288 nm for chloranil and 262 nm for PDNB). The amount adsorbed was calculated from the difference in the absorbance, before and after adsorption.

2.4. Catalytic activity studies

The oxidative dehydrogenation experiments were carried out in a fixed-bed down flow silica reactor (20 mm ID), with a provision for passing dry air (10 mL/min) along with ethylbenzene. The catalyst was placed at the center of the reactor. The materials were pretreated for 12 h at 773 K under air and brought down to the reaction temperature by cooling under a current of nitrogen gas of high purity. The feed was delivered using a syringe pump (ISCO model 500 D). Liquid and gaseous products were collected and separately analyzed using GC fitted with a xylene master capillary column and flame ionization detector. The liquid mass balance for all the experiments was above 98 wt%, with a relative error of ±2%. The

Table 1
Chemical analysis, XRD parameter, surface area and textural properties of $Cu_{1-x}Co_xFe_2O_4$

Catalyst composition (x)	Metal concentration (wt.%)[a]			Crystallite size (nm)	a (Å)	Specific surface area (m^2/g)	Micorpore surface area (m^2/g)	Total pore volume (cc/g) (10^{-3})	Average pore diammeter (Å)
	Co	Cu	Fe						
0.0	–	27.1	46.2	15.25	8.3898	28.8	3.0	51.0	33.24
0.25	6.1	20.2	46.7	13.85	8.4051	34.0	7.8	66.7	33.47
0.50	12.4	13.5	47.1	13.17	8.4012	43.8	10.2	108.6	32.73
0.75	18.6	6.9	47.3	14.77	8.3982	36.6	4.3	63.6	33.34
1.0	25.1	–	47.6	14.13	8.3997	36.8	6.9	59.4	33.37

[a]Chemical analysis results obtained from XRF.

negligible amount of CO_x and ethylene were observed in all the studied cases.

3. Results and discussion

3.1. General characterization

Figure 1 shows the XRD patterns of the calcined catalysts. All the samples exhibited the typical XRD patterns of cubic spinel structure with peaks for 111, 220, 311, 222, 400, 422, 511 and 440 planes falling at "*d*" values of 4.89, 2.97, 2.53, 2.42, 2.08, 1.71, 1.61 and 1.48 Å respectively. However, the diffractograms of $CuFe_2O_4$ shows additional peaks characteristic of α-Fe_2O_3 and CuO phases, indicating that spinel formation is not complete at 773 K for $x = 0$. Addition of cobalt results in the formation of a more uniform structure, and the additional reflections seen in the previous case are hardly detected at the $x \neq 0$ compositions. The lattice constants, "*a*", calculated for $CuFe_2O_4$ and $CoFe_2O_4$ are 8.3898 and 8.3997 Å respectively, and they are in good agreement with the literature values [20–22]. The broad peaks seen in XRD indicates the fine particle size of the ferrite formed due to coprecipitation in contrast to the sharp peaks reported for materials prepared by the ceramic method. The fine particle size of the ferrite is also evident from the crystallite size of 13 to 16 nm for all samples estimated from the most intense peak (311) using the Debye–Scherrer equation [23].

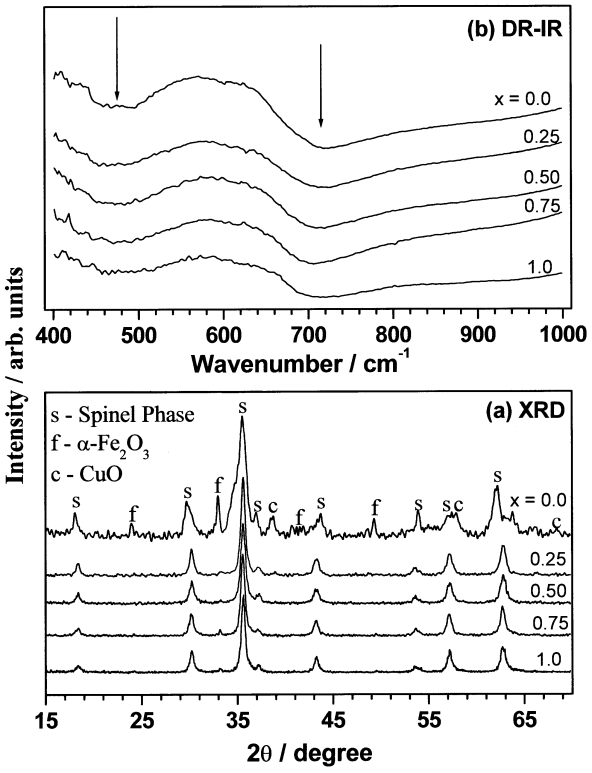

Figure 1. (a) X-ray diffractograms and (b) diffuse reflectance IR (DR-IR) of $Cu_{1-x}Co_xFe_2O_4$ samples recorded at room temperature after calcination at 500 °C. Arrows in DR-IR indicate ν_{M-O} of T_d (710 cm^{-1}) and O_h (460 cm^{-1}) coordinated cations.

The results obtained from surface area analysis of $Cu_{1-x}Co_xFe_2O_4$ are summarized in table 1. N_2-adsorption isotherms of all these compositions are of mixed type. N_2-adsorption–desorption isotherms for a representative composition $x = 0.50$ is shown in figure 2. There is a gradual rise in the volume depicted by all the curves with increasing relative pressure (P/P_0). At around $P/P_0 = 0.8$, a rapid rise in volume is observed. Thus, these isotherms represent the combination of type IV and type II nature. The isotherms of type IV indicate the presence of mesoporosity present in the samples. The peak-to-peak diameter of the mesopores is around 33 Å for all the compositions indicating uniformity of the pores in the mesopore range. The external surface area obtained from the de Boer *t*-plots exceeds the 75% values of the BET surface area of the individual compositions, further confirming the presence of mesoporosity in the samples. The fraction of the micropore volume per total pore volume is less than 6% for all the compositions calcined at 773 K.

Figure 1 shows the diffuse reflectance IR spectra of the ferrite samples recorded between 400 cm^{-1} and 1000 cm^{-1}. All compositions of the system showed two strong IR bands ν_1 and ν_2, around 710 and 460 cm^{-1}, respectively. Vibration of the T_d metal-oxygen group corresponds to the highest restoring force and is thus assigned to the highest frequency band (i.e. at 710 cm^{-1}), and the band at 460 cm^{-1} indicates the vibration of the Oh metal-oxygen group [24–27]. According to Waldron [26], the tetrahedral coordination has the effect of substantially increasing the frequency of vibration, since these cations introduce a supplementary restoring force in a preferential direction along the M_{Tet}–O bond. The broad absorption bands for $Cu_{1-x}Co_xFe_2O_4$ indicate the inverse nature of spinel for all the compositions. The important physicochemical characteristics of $Cu_{1-x}Co_xFe_2O_4$ calcined at 773 K are presented in table 1. A detailed account of the physicochemical characteristics of $Cu_{1-x}Co_xFe_2O_4$ is already reported elsewhere [19,28,29].

3.2. Acid-base properties

The IR spectrum of pyridine adsorbed on $Cu_{1-x}Co_xFe_2O_4$ at 373 K is shown in figure 3. The most intense bands appeared at 1606, 1485 and 1446 cm^{-1} (ν_{8a}, ν_{19a} and ν_{19b} ring vibrations), indicating Lewis acidity. Trace amount of Brønsted acid sites are present, indicated by a small peak at 1541 cm^{-1}. However, the main contribution of acidity is due to Lewis acid sites. A detailed description of the acid–base properties of the presently studied catalyst system is already reported separately [19]. There is a linear dependence between cobalt content and Lewis acidity.

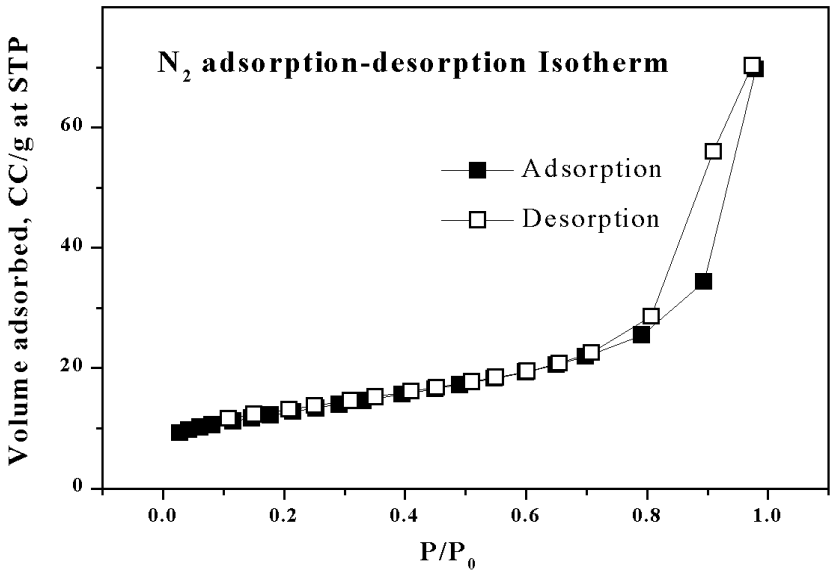

Figure 2. N_2 adsorption–desorption isotherm curve obtained from surface area measurement for the composition $x = 0.50$.

In other words, the intensity of bands was directly proportional to "x", i.e., the higher the cobalt content the stronger the Lewis acidity.

The ν_{8a} band position at 1606 cm^{-1} indicates that the contribution to pyridine adsorption of Oh cations is larger than that of Td ions [19 and references therein]. In other words, octahedral cations are mainly exposed on the surface of $Cu_{1-x}Co_xFe_2O_4$. Recent works based on advanced surface analysis techniques such as low-energy ion scattering (LEIS), a technique used for identifying the surface atomic layer of solid surfaces [30], have revealed that the outermost atomic layer of spinels contains mainly Oh cations, which is an evidence for our result. Also, by considering the polarizing power and statistical distribution of cations, it can be assumed that, among these surface Oh sites, Fe^{3+} prevails over Co^{2+} and Cu^{2+} and consequently contributes more toward the pyridine adsorption and the imparting of Lewis acidity. This is further supported by increasing the $Fe/(Cu + Co)$ surface atomic ratio from 0 to 1, calculated from XPS analysis (table 2) [29]. Though the polarizing power of iron is far greater than that of cobalt or copper, the stabilizing effect of cobalt on the distribution of iron sites can be proposed as the reason for the strengthening of the acidity.

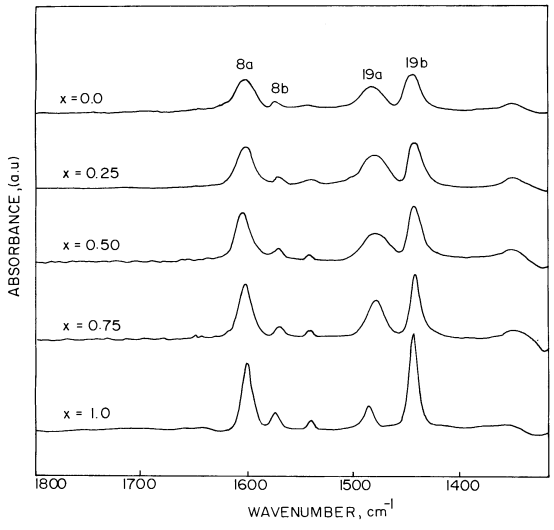

Figure 3. FTIR spectra of pyridine adsorbed on $Cu_{1-x}Co_xFe_2O_4$ surfaces at 373 K, after *in situ* activation at 673 K.

IR spectrum of CO_2 adsorbed on $Cu_{1-x}Co_xFe_2O_4$ at 298 K is shown in figure 4. Asymmetric stretching of adsorbed CO_2 and carbonate vibrations are observed at 2400–2300 cm^{-1} and 1800–1200 cm^{-1} respectively [31–33]. Two sharp bands observed in the range 2400–2300 cm^{-1} are due to the coordination of CO_2 on the surface Lewis acid sites. Three broadbands observed in the range 1800–1200 cm^{-1} demonstrate the various types of carbonate vibrations, and measure the surface basicity. The interpretation of these different carbonate vibrations is described in our earlier publication [19]. The intensity of various bands observed between 1800 and 1200 cm^{-1} generally decreases with increasing x, indicating a decrease in basicity from $x = 0$ to 1. Moreover, the width and intensity of the carbonate vibrations suggests that the bidentate mode seems to be

Table 2
Surface atomic ratio (from XPS) and limiting values of electron acceptors (EA) adsorbed over $Cu_{1-x}Co_xFe_2O_4$

Catalyst composition (x)	Limiting amount of EA adsorbed ($\times 10^{-4}$ mmol/m^2)		Fe/(Cu + Co) Surface atomic ratio from XPS
	TCNQ	Chloranil	
0.00	45.56	21.03	0.85
0.25	41.70	14.11	0.81
0.50	31.63	9.26	0.90
0.75	26.35	6.85	1.00
1.00	21.46	5.80	1.33

the dominant adsorption state on $Cu_{1-x}Co_xFe_2O_4$ and indicates the presence of coordinatively unsaturated ions.

Although we accept that the diffuse reflectance is qualitative, we have used the relative value of acidity/basicity rather than absolute value for the comparison. Also, the relative value presented here is after the normalization with surface area, which ensures minimum error. Also, the electron donor/acceptor properties of the catalyst system reveal a linear correlation between the copper content and basicity [19]. This substantiates the information from FTIR adsorption of CO_2. A detailed description of acid–base properties of $Cu_{1-x}Co_xFe_2O_4$ is published elsewhere [19].

Adsorption studies of three electron acceptors (EAs), namely, 7,7,8,8-tetracyanoquinodimethane (TCNQ), 2,3,5,6-tetrachloro-1,4-benzoquinone (chloranil) and *p*-dinitrobenzene (PDNB) with electron affinity values 2.84, 2.40 and 1.77 eV, respectively, were performed on $Cu_{1-x}Co_xFe_2O_4$. The Langmuir type of adsorption isotherms are plotted for TCNQ and chloranil (figure 5) for calculating the limiting amounts adsorbed; the values are presented in table 2 (the limiting concentrations were expressed in mmol/m^2; the surface areas being determined using the BET method for each sample). TCNQ being a strong EA (electron affinity value 2.84 eV), its anion radicals are expected to form on the strong as well as weak basic sites, whereas chloranil with an intermediate electron affinity value (2.40 eV) cannot accept electrons from very weak donor sites. The negligible adsorption of PDNB (electron affinity value 1.77 eV) for all systems indicates the absence of very strong donor sites, and hence, the limiting amount of TCNQ and chloranil would be an estimate of the weak or moderate basic sites. This demonstrates that the adsorption sites on Cu–Co ferrites act as electron donors to the adsorbed molecule with electron affinity values <1.77 eV. EA adsorption studies indicate that the basicity of the $Cu_{1-x}Co_xFe_2O_4$ system decreases with increasing x. Thus, Cu-rich compositions possess a large number of strong and moderately strong donor sites.

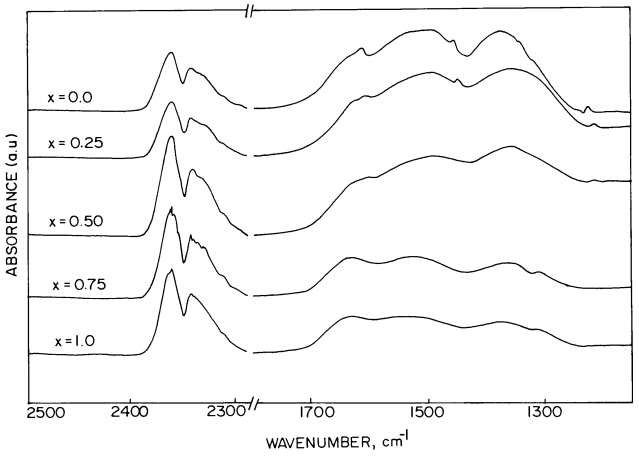

Figure 4. FTIR spectra of CO_2 adsorbed on $Cu_{1-x}Co_xFe_2O_4$ at room temperature (298 K).

3.3. Acid–base strength and ethylbenzene dehydrogenation activity

The reaction of ethylbenzene to styrene is endothermic with $\Delta H = 124.9$ KJ/mol. Hence, an increase in temperature will always favor the reaction. However, in the present system, styrene selectivity increased first in the temperature range of 648 to 698 K and thereafter it decreased because of the increased rate of side reactions like disproportionation and dealkylation reaction at high temperature, as represented by figure 6.

The product distribution and selectivity data of the oxidative dehydrogenation of ethylbenzene over the catalyst system under the optimized conditions are presented in table 3. As can be seen, styrene is the main product with benzene and toluene as minor products, no matter whether the results were recorded at the initial or steady state. There is a rising trend in the conversion and selectivity of styrene as x decreases from 0 to 0.50 and thereafter decreases.

The influence of the Cu–Co combination is a factor decisive to ethylbenzene conversion, and styrene

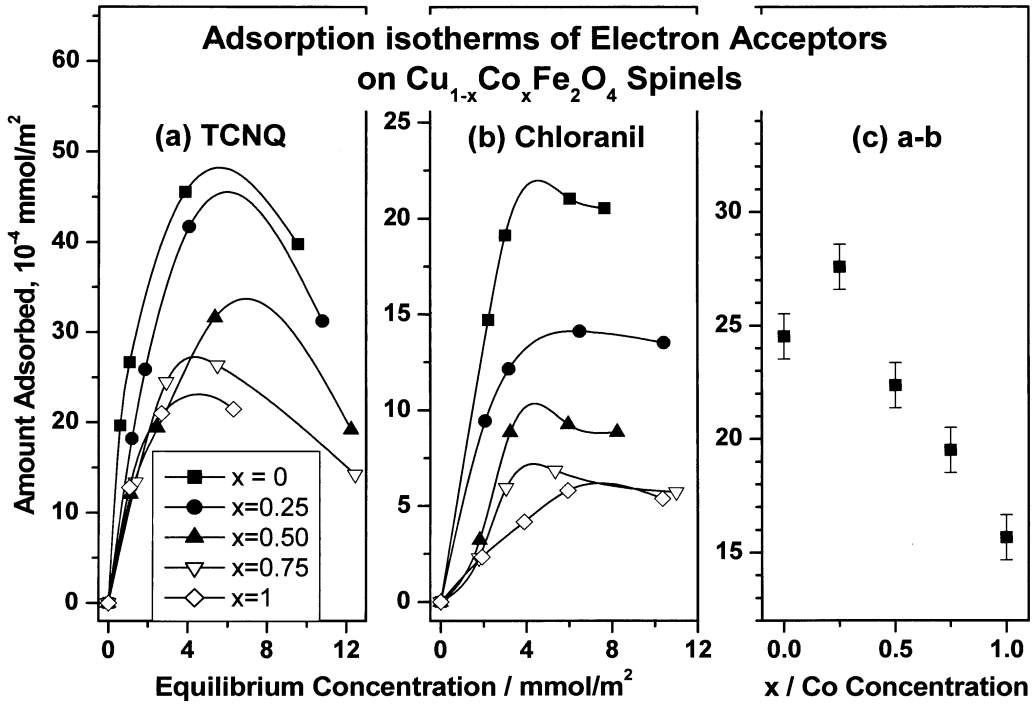

Figure 5. Adsorption isotherms of (a) TCNQ and (b) chloranil in acetonitrile on $Cu_{1-x}Co_xFe_2O_4$ system calcined at 773 K. The difference between the limiting amounts of TCNQ and chloranil adsorbed at each composition is shown in (c).

selectivity is evident from the following results:

1. Both ethylbenzene conversion and styrene selectivity increases from end compositions ($x = 0$ and 1) to intermediate compositions.
2. Among various intermediate compositions, $x = 0.50$ shows maximum activity in terms of ethylbenzene conversion and styrene selectivity. This indicates that an equal amount of copper and cobalt is necessary in the bulk for effective reaction.

The activity observed is not because of an apparent correlation between surface area and ethylbenzene conversion. A similar reaction pattern was observed for phenol alkylation reaction over the same catalysts compositions reported earlier [28,29]. Also, we would like to mention here that the surface area of $Cu_{1-x}Co_xFe_2O_4$ system prepared by high-temperature glycine nitrate combustion method [29], exhibits $<2\,m^2/g$ for all compositions and shows low methylation activity but follows the same trend as that of the samples prepared by coprecipitation. In other words, the intermediate composition shows better catalytic performance than the other compositions. The same reaction pattern can be seen in the present study also. Thus, we strongly believe that it is the combination of copper and cobalt that govern the activity rather than the surface area and this is well proven in our previous study. Replacement of copper by cobalt modifies the acid/base sites that govern the activity.

The analysis of the spent catalysts by XRD revealed trace amounts of copper, which indicates that the catalysts are partially reduced. However, the extent of

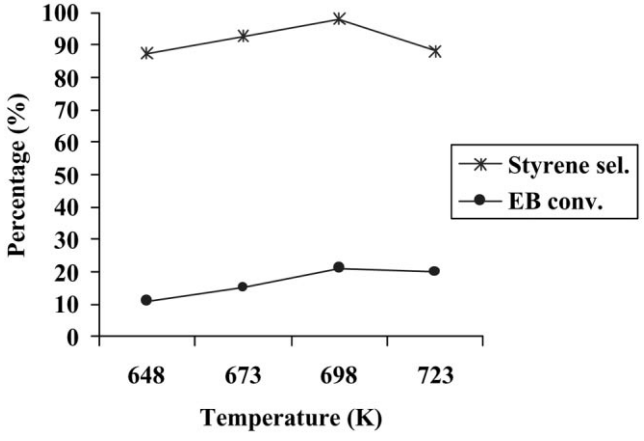

Figure 6. Effect of temperature over $Cu_{0.50}Co_{0.50}Fe_2O_4$ catalyst.

Table 3
Product distribution and selectivity data for the oxidative dehydrogenation of ethylbenzene over $Cu_{1-x}Co_xFe_2O_4$

Product distribution (Mol %)	Catalyst composition (x)				
	0	0.25	0.50	0.75	1
Benzene	0.75	0.85	0.32	1.71	2.37
Toluene	0.18	0.56	0.08	0.27	0.59
Ethylbenzene	94.53	88.86	79.04	85.56	89.76
Styrene	4.53	10.74	20.56	11.46	7.27
EB conversion	5.46	11.15	20.96	13.44	10.24
Styrene selectivity	82.97	87.43	98.09	85.27	70.99

Note: Reaction temperature = 698 K, WHSV = $1\,h^{-1}$ and TOS = 3 h.

reduction decreases as the cobalt content increases, which follows the same trend as that observed in the TPR reported previously [28].

On the basis of the facts discussed above, we are able to conclude that the oxidative dehydrogenation activity of $Cu_{1-x}Co_xFe_2O_4$ catalysts can be interpreted in connection with their acid-base properties, which are strongly changed by the catalyst composition. Figure 7 displays a comparison between the catalytic performance in terms of EB conversion and selectivity to styrene obtained at a reaction temperature of 698 K and relative acidity (and basicity) obtained from the area of the ν_{8a} and ν_{19b} bands (bands between 1700 and 1200 cm^{-1}) in the FTIR spectra of pyridine (CO_2) adsorbed on the catalysts. It is to be noted here that Brønsted acid sites are not considered, as they are too weak and the relative acidity and basicity given in figure 7 is qualitative.

It is interesting to note that: (1) although the binary oxide $CuFe_2O_4$ had a large amount of basic site, it only showed the median activity because of its low acidity, and (2) the binary oxide, $CoFe_2O_4$, which had a great amount of acidic site along with a small amount of basic site, also showed the median activity. However,

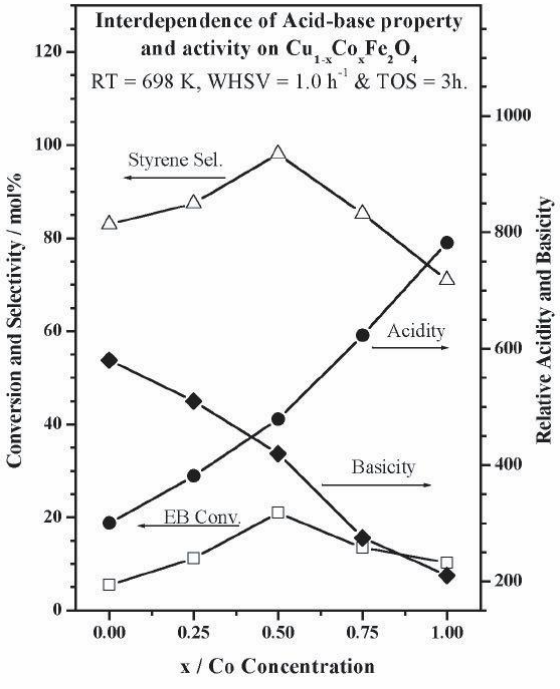

Figure 7. A comparison between the catalytic performance (Ethylbenzene conversion and selectivity of styrene), and relative acidity obtained from the area of the ν_{8a} and ν_{19b} bands in FTIR spectra of pyridine adsorbed on $Cu_{1-x}Co_xFe_2O_4$ catalysts at 373 K and the relative basicity obtained from the area of the bands between 1700 and 1250 cm^{-1} from CO_2 adsorbed on $Cu_{1-x}Co_xFe_2O_4$ catalysts at 298 K. Note the good correlation between the intermediate acid–base property and high catalytic activity.

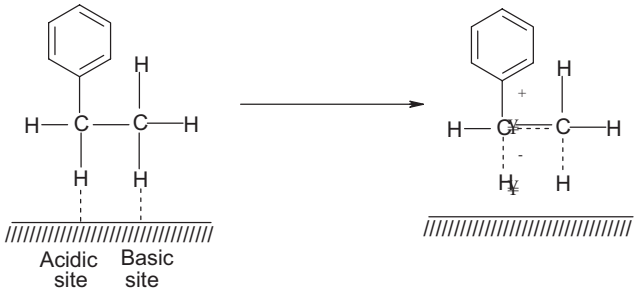

Figure 8. Adsorption of ethylbenzene over $Cu_{1-x}Co_xFe_2O_4$ facilitated by the bifunctional nature of the surface.

intermediate compositions show better catalytic performance, among which $x = 0.50$ is superior and demonstrates an intermediate acid–base character. Since $Cu_{0.50}Co_{0.50}Fe_2O_4$ catalyst was prepared for a good acid–base balance, the EB conversion and the selectivity to styrene were maintained without the rapid change during the reaction, and the selectivity to styrene was very high. Also, the deactivation of catalyst was not observed during the reaction. This can be explained in terms of the reaction mechanism of ethylbenzene dehydrogenation proposed by Wang *et al*. [7]. According to this mechanism, the dehydrogenation of EB over these oxides also proceeds by the acid–base bifunctional mechanism, in which α-H of ethylbenzene attacks the acid site of the catalyst, and simultaneously the β-H attacks the basic site of the catalyst as shown in figure 8. The partial positive charge on the α-C of transition state could be stabilized by the aromatic ring. Therefore, the active sites balanced with acidic and basic sites must be present on the catalyst. Thus, the balance of acid–base property is very important for an efficient ethylbenzene dehydrogenation.

The formation of toluene and benzene during the oxidative dehydrogenation reaction is caused by the interaction of acid–base centers on the catalyst surface as reported by Wang *et al*. [7] and Krouse *et al* [34]. Strong basic sites can abstract the β-H of the adsorbed ethylbenzene, which facilitates the cleavage of side chain C–C bond resulting in the formation of toluene, whereas strong acidic centers can abstract α-H of ethylbenzene and facilitates the cleavage of phenyl–C bond, resulting in the high yield of benzene [7,34]. However, the formation of benzene and toluene require relatively high temperature and in the present system large amount of benzene and toluene were formed at 773 K with high ethylbenzene conversion and comparatively low styrene selectivity (results not shown). Thus, the present catalyst system, specifically $x = 0.50$ composition is very active even at low temperature in comparison with our earlier reported Zn–Ni ferrite system [18]. From our results, it is certain that $x = 0.50$ catalyst brings out a combined effect or sort of synergistic behavior enhancing the catalytic activity. Furthermore, it is believed that the acidic and basic character of the

catalysts would affect the product selectivity. It has already been shown from our earlier XPS results [29] on $Cu_{1-x}Co_xFe_2O_4$ that the $x = 0.50$ composition exhibits Cu–Co synergism that is correlated with the catalytic performance, which is very much evidenced in the present study also.

4. Conclusions

A series of ferrospinels having the general composition $Cu_{1-x}Co_xFe_2O_4$ ($x = 0$, 0.25, 0.50, 0.75 and 1) was prepared by a coprecipitation method and characterized by XRD, XRF, FTIR and surface area. Acid–base properties were studied in detail by FTIR adsorption of pyridine and CO_2 as well as by adsorption studies.

The FTIR spectrum of pyridine-adsorbed $Cu_{1-x}Co_xFe_2O_4$ surfaces at 373 K demonstrates that the predominant modes of adsorption are ν_{8a} and ν_{19b}, and bolstering the dominant Lewis acid character. As for the dependence on the composition, the intensity of the bands was directly proportional to x, i.e., the higher the cobalt content the stronger the Lewis acidity. However, the polarizing power of iron is far greater than that of cobalt or copper; thus the stabilizing effect of cobalt on the distribution of iron sites can be proposed as the reason for the strengthening of the acidity. CO_2 adsorption as well as adsorption studies of electron acceptors such as 7,7,8,8-tetracyanoquinodimethane, 2,3,5,6-tetrachloro-1-4-benzoquinone and *p*-dinitrobenzene on $Cu_{1-x}Co_xFe_2O_4$ indicate that the basicity of the system decreases with increasing x.

The oxidative dehydrogenation of EB over $Cu_{1-x}Co_xFe_2O_4$ indicates that both ethylbenzene conversion and styrene selectivity increases from end compositions ($x = 0$ and 1) to intermediate compositions and among various intermediate compositions, $x = 0.50$ shows the maximum activity in terms of ethylbenzene conversion and styrene selectivity. The activation of the reactant molecule is associated with an acid–base-type interaction between the reactant molecule and metal oxide and this function plays a determining role in the catalytic activity and selectivity of ethylbenzene dehydrogenation. Among the various compositions, $Cu_{0.50}Co_{0.50}Fe_2O_4$ exhibits good acid–base balance, the EB conversion and the selectivity to styrene were maintained without the rapid change during the reaction, and the selectivity to styrene was very high.

Acknowledgment

Thomas Mathew and Shivanand Pai are grateful to CSIR, New Delhi, for awarding research fellowships.

References

[1] E.H. Lee, Catal. Rev. 8 (1973) 285.
[2] B. Delmon, P.A. Jacobs and G. Poncelet, *Preparation of Catalysts II* (Elsevier, Amsterdam, 1979) pp. 293–305.
[3] D.E. Stobbe, F.R. Van Buren, M.S. Hoogenraad, A.J. Van Dillen and J.W. Geus, J. Chem. Soc., Faraday Trans. 87 (1991) 1639.
[4] F.J. O'Hara, U.S. Patent 3,904,552 (1975).
[5] T. Hirano, Appl. Catal. 28 (1986) 119.
[6] J-H. Wu, C-S. Chwg and I. Wang, Appl. Catal. 18 (1985) 295.
[7] I. Wang, W-F. Chang, R-J. Shiau, J-C. Wu and C-S. Chung, J. Catal. 83 (1983) 438.
[8] I. Wang, J-C. Wu and C-S. Chung, Appl. Catal. 16 (1985) 89.
[9] H.H. Kung and M.C. Kung, J. Phys. Chem. 84 (1980) 383.
[10] W.L. Kehl and R.J. Rennard, U.S. Patent 3,450,787 (1969).
[11] R.J. Rennard and W.L. Kehl, J. Catal. 21 (1971) 282.
[12] S. Velu, K. Suzuki, M. Okazaki, M.P. Kapoor, T. Osaki and F. Ohashi, J. Catal. 194 (2000) 373.
[13] E.J.W. Verwey and E.L. Herlman, J. Chem. Phys. 15 (1947) 174.
[14] K. Balasubramanian and V. Krishnasamy, Indian J. Chem. 21A (1982) 813.
[15] W.S. Chen, M.D. Lee and J.F. Lee, Appl. Catal. 83 (1992) 201.
[16] C.S. Narasimhan and C.S. Swamy, Appl. Catal. 2 (1982) 315.
[17] M. John Jebarathinam, M. Eswaramoorthy and V. Krishnasamy, Appl. Catal. A: Gen. 145 (1996) 57.
[18] K. Sreekumar, M. Thomas, T.M. Jyothi, M.D. Biju, S. Suganan and B.S. Rao, Polish J. Chem. 74 (2000) 509.
[19] T. Mathew, N.R. Shiju, B.B. Tope, S.G. Hegde, B.S. Rao and C.S. Gopinath, Phys. Chem. Chem. Phys. 4 (2002) 4260.
[20] E. Prince and R.G. Treuting, Acta. Crystallogr. 9 (1956) 1025.
[21] J. Smith and H.P.J. Wijn, Adv. Electron. Electronphys. 6 (1954) 83.
[22] G.H. Jonker, J. Phys. Chem. Solids 9 (1959) 165.
[23] N.F.M. Henry, J. Lipson and W.A. Wooster, *The Interpretation of X-Ray Diffraction Photographs* (Macmillan and Co Ltd., London, 1951).
[24] P. Tarte, Spectrochim. Acta. 19 (1965) 49.
[25] J. Preudhomma and P. Tarte, Spectrochim. Acta, Part A 27 (1971) 961.
[26] R.D. Waldron, Phys. Rev. 99 (1955) 1727.
[27] W.B. White and B.A. De Angelis, Spectrochim Acta, Part A 23 (1967) 985.
[28] K. Lázár, T. Mathew, Z. Koppány, J. Megyeri, V. Samuel, S.P. Mirajkar, B.S. Rao, and L. Guczi, Phys. Chem. Chem. Phys. 4 (2002) 3530.
[29] T. Mathew, N.R. Shiju, K. Sreekumar, B.S. Rao and C.S. Gopinath, J. Catal. 210 (2002) 405.
[30] J.P. Jacobs, A. Maltha, J.R.H. Reintjes, T. Drimal, V. Ponec and H.H. Brogersma, J. Catal. 147 (1994) 294.
[31] R. Philipp and K. Fujimoto, J. Phys. Chem. 96 (1992) 9035.
[32] K. Nakamoto, *Infrared and Raman Spectra of Inorganic and Coordination Compounds*, 3rd ed. (Wiley, New York, 1978) p. 243.
[33] C. Morterra, G. Ghiotti, F. Boccuzzi and S. Coluccia, J. Catal. 51 (1978) 299.
[34] A. Krause, Sci. Pharm. 38 (1970) 266.